Control of Non-metallic Inclusion Plasticity and Steel Cleanliness for Ultrathin 18 Pct Cr-8 Pct Ni Stainless Steel Strip

JING GUO, SHAOWEI HAN, XINGRUN CHEN, HANJIE GUO, and YAN YAN

Laboratory-scale slag-steel equilibrium experiments as well as thermodynamic analyses and industrial tests were performed for 18 pct Cr-8 pct Ni stainless steel to study the effect of slag composition on non-metallic inclusion plasticity and steel cleanliness. First, the results showed that saturated MgO should be added in refining top slag, in particular for low-basicity slag, to avoid heavy corrosion of the refractory lining. Further, the content of MgO + Al_2O_3 increased and MnO content decreased in inclusions with an increase in the slag basicity; thus, the plasticity of inclusions decreased correspondingly. Conversely, higher-basicity slag was favorable for reducing the total oxygen (T.O.), while the content of dissolved aluminum (Als) in steel increased. On the basis of experimental results and thermodynamic analyses, it was concluded that comprehensive favorable inclusion plasticity and relatively high steel cleanliness could be achieved for slag basicity (CaO/SiO_2) in the range of 1.4 to 1.8 and Als lower than 10 ppm. This was verified by industrial test results.

https://doi.org/10.1007/s11663-020-01862-4

I. INTRODUCTION

OWING to its outstanding anticorrosion and comprehensive mechanical properties, ultrathin stainless steel strips (thinner than 0.2 mm) are being increasingly applied in many fields such as medical apparatuses and instruments, electronic products, food equipment, aerospace, and the aircraft industry. However, one of most significant challenges in manufacturing ultrathin stainless steel strips is that it is much more difficult to control the surface quality because non-metallic inclusions are more likely to be exposed on the strip surface when the strip thickness decreases. Hence, the characteristics of inclusions such as the size, number, distribution, and hardness significantly influence the surface quality of ultrathin stainless steel strips.

It is generally agreed that inclusions with a low melting point can be deformed during the rolling process, and surface defects caused by non-inclusions can be effectively reduced.[1,2] The deformability of the inclusions was verified to be closely related to their chemical composition.[3–7] There are two main types of non-metallic inclusions in Si-killed 300-type stainless steel: a $CaO-SiO_2-Al_2O_3$-based system and a $MnO-SiO_2-Al_2O_3$-based system.[1,2,8] They have very different properties and effects on the surface quality of stainless steel strips. Many researchers have studied methods of controlling the composition of the inclusions.

Yang *et al.*[9] achieved a low melting point of inclusions in spring steel in industrial production by adjusting the composition of $CaO-SiO_2-Al_2O_3-MgO$ refining slag. Wang *et al.*[10] found that increasing the basicity of $CaO-SiO_2-Al_2O_3$-based top slag was beneficial to the cleanliness of Fe-13Cr stainless steel, but a basicity over 2.58 led to a high content of [Al] in liquid steel, which promoted the formation of $MgO-Al_2O_3$ inclusions. Park *et al.*[11] studied the effects of slag composition on the concentration of Al_2O_3 for inclusions in Si-Mn-killed steel, and found that the (mol pct MnO)/(mol pct SiO_2) of the inclusion composition was mainly equal to 0.8 (± 0.06) when the Al_2O_3 content in inclusion was increased from about 10 to 40 mol pct by increasing the basicity of the slag from about 0.7 to 2.1. Wijk *et al.*[12] investigated the purity of ferrosilicon and its influence on the inclusion cleanliness of steel, and pointed out that an increased content of aluminum resulted in the formation of alumina inclusions.

JING GUO, HANJIE GUO, and YAN YAN are with the School of Metallurgical and Ecological Engineering, University of Science and Technology Beijing (USTB), Beijing 100083, China. Contact e-mail: guojing@ustb.edu.cn SHAOWEI HAN is with the Steelmaking Department, Beijing Shougang Co., Ltd, Qian'an, 064400, Hebei, China. XINGRUN CHEN is with the State Key Laboratory of Advanced Metallurgy, University of Science and Technology Beijing (USTB), Beijing 100083, China and also with the Hongxing Iron & Steel Co. Ltd., Jiuquan Iron and Steel Group Corporation, Jiayuguan, 735100, Gansu, 735100, China.

Manuscript submitted December 27, 2019.
Article published online May 26, 2020.

Meanwhile, high-purity ferrosilicon resulted in the formation of silicates that were removed more slowly from the melt. Kang *et al.*[13] found that important factors in determining the liquidus temperature and primary phase of the inclusions are the MnO/SiO_2 ratio and Al_2O_3 content in the inclusions of Si/Mn deoxidized steel. He also reported that through proper design of low-basicity top slag composition, the inclusions showed a low liquidus temperature and soft primary phase. Ren *et al.*[14] reported that when low-basicity slag was employed for refining, inclusions with a low melting point $MnO\text{-}SiO_2\text{-}Al_2O_3$ system could be obtained, the content of total oxygen (T.O.) in steel increased, and the content of dissolved aluminum (Als) decreased. By contrast, when high-basicity refining slag was employed, the inclusions were an $Al_2O_3\text{-}CaO\text{-}SiO_2$ system, and the melting point of the inclusions increased when the content of T.O. in steel decreased.

In summary, lower-basicity refining slag should be applied to Si-killed 18 pct Cr-8 pct Ni stainless steel to obtain low melting inclusions. However, in the actual production process, the refractory lining of the refining furnace is typically made of MgO-C-based material, and thus the low-basicity refining slag may cause heavy erosion of the lining. Therefore, it is necessary to consider how to prevent the erosion of the lining, in particular, when low-basicity refining slag is applied. Furthermore, in many cases, not only favorable non-metallic inclusion plasticity but also relatively high steel cleanliness is required in ultrathin stainless steel strips. These aspects are still not well understood up to now.

Accordingly, careful and comprehensive investigations were carried out to illuminate these issues in this paper. Firstly, pre-experiments were performed to expound how to prevent refractory-lining corrosion in the case of low-basicity slags in a laboratory. Secondly, slag-steel equilibrium experiments with refining slags of different basicities are carried out to investigate the effect of slag basicity on the plasticity of inclusions and steel cleanliness under the premise of ensuring that the slag almost does not erode the lining. Further, a quantitative thermodynamics interpretation of the changes in the T.O. and Als in steel is performed using the ion-molecule coexistence theory and the thermodynamic software FactSage. Finally, industrial tests are carried out to verify the laboratory experimental and thermodynamic calculated results.

II. EXPERIMENTAL DETAILS

A. *Laboratory-Scale Experiments*

First, a series of pre-experiments were carried out to understand the prevention of refractory-lining corrosion when low-basicity slags are applied. Three heats of experiments were carried out in a vertical electric resistance furnace with two MoSi heating bars under an Ar atmosphere. The synthetic slags were a mixture of analytically pure-grade powders of CaO, SiO_2, MgO, Al_2O_3, and CaF_2 and commercial 18 pct Cr-8 pct Ni stainless steel was applied as mother alloy in the present experiments. The compositions of the initial slag and 18 pct Cr-8 pct Ni stainless steel are shown in Tables I and II, respectively. The content of MgO in the initial slags (marked as M1, M2, and M3) was 0 pct, 5 pct, and 10 pct, respectively, and the CaF_2 content in the slag was approximately 20 pct. The basicity of the initial slag was constant at 1.4.

During the experiments, 100 g of stainless steel and 20 g of synthetic slag were placed in a MgO crucible having a 45 mm inner diameter and a 120 mm depth. The temperature was increased at 10 K/min in an argon atmosphere with a flowrate of 1.5 L/min. After the furnace temperature rose to 1823 K(1550 °C), it was maintained for 2 h to ensure slag-steel reactions in equilibrium.[15,16] Thereafter, the MgO crucible was taken out and quenched in air after the reaction. In the present study, the change of MgO content in the slag before and after the reaction reflected the amount of the actual refractory-lining erosion.

Next, six groups of steel-slag equilibrium experiments with slags of different basicities were carried out on the basis of pre-experimental results. The basicity of the slag varied from 1.0 to 3.0. The content of Al_2O_3 in the initial slag was about 2 pct, and the original composition of the refining slag is shown in Table III. In the present experiments, the MgO content in the initial slag was assigned as its corresponding saturation content calculated using the FactSage 7.2 with database FactPS and Ftoxid[17] on the basis of the pre-experimental results. It should be pointed out that the contents of MgO in the R5 and R6 slag systems were adjusted to 2.5 pct since they have a very low content of saturated MgO.

The steps of these experiments were the same as those of the pre-experiments. After each experiment, steel and slag in the crucible were separated from each other. The steel sample was sectioned into two parts: one for a chemical analysis and the other mounted and polished for non-metallic inclusion determination by an automated inclusion analyzer (EVO18, Zeiss, German). The instrument was operated at an accelerated voltage of 20 kV, step size of 3 pot and a magnification of 1300 times, under which the minimum detected inclusion size was approximating 1.0 μm and the resolution was 1024; non-metallic inclusions were detected by backscattered electron imaging. The analyzed area per sample was 5 mm $\times$ 5 mm. It should be pointed out Fe, Cr and Ni in the inclusion detected by energy disperse spectroscopy (EDS) were removed to minimize the effects of steel matrix on inclusion composition and some unclear spots detected were selected and excluded before the present inclusion analysis. The composition of the slag was determined by an X-ray fluorescence (XRF) spectrometer. The Als content of the steel was analyzed by inductively coupled plasma mass spectrometry (ICP-MS). The T.O. and N in the steel was analyzed using a Leco O/N analyzer.

Table I. Composition of Initial 18 Pct Cr-8 Pct Ni- Stainless Steel, Mass Pct

C	Si	Mn	P	S	Cr	Ni	T.O.	Als	N
0.05	0.41	1.20	0.03	0.001	18.01	8.02	0.0030	0.0010	0.042

Table II. Composition of Initial Slag in Pre-experiments, Mass Pct

No.	CaO	SiO_2	CaF_2	MgO	MgO* (1823 K)
M1	46.67	33.33	20	0	11.91
M2	43.75	31.25	20	5	11.3
M3	40.83	29.17	20	10	10.6

MgO* represents MgO saturation in corresponding slag calculated by FactSage software.

Table III. Composition of Initial Slag in Steel-Slag Equilibrium Experiments, Mass Pct

No.	R	CaO	SiO_2	CaF_2	Al_2O_3	MgO
R1	1.0	31.47	31.47	16.14	1.61	19.31
R2	1.4	40.44	28.89	17.78	1.78	11.12
R3	1.8	47.38	26.32	18.90	1.89	5.51
R4	2.2	52.29	23.77	19.50	1.95	2.50
R5	2.6	47.31	18.19	30.00	2.00	2.50
R6	3.0	49.13	16.38	30.00	2.00	2.50

B. *Industrial Tests*

On the basis of laboratory-scale experimental results and thermodynamic analyses, industrial tests were carried out in a commercial stainless steel plant in P.R. China. The manufacturing processes of testing heat were followed by 110-ton argon-oxygen-degassing (AOD) ladle-furnace (LF) continuous casting (CC). Proper amounts of light-burning dolomite and silica were added to the LF to adjust the slag basicity to approximately 1.5 and to avoid heavy erosion to the ladle lining (T1). In addition, another heat (marked as T2) with conventional higher-basicity (about 1.8) slag was also carried out in the same process, in which a normal ferrosilicon with aluminum content about 1.3 pct was applied. It should be pointed out that other parameters, such as the initial composition of hot metal, smelting temperature and time, heat treatment temperature and time, were kept similar level between the two heats as much as possible to exclude their disturbances to the inclusion composition and steel cleanliness. Steel samples at central, 1/4 and edge position of central line along the width direction within one slab of heat T1 and T2 were taken out for inclusion observation.

III. RESULTS AND DISCUSSION

A. *Effect of MgO Content in Low-Basicity Slag on MgO Crucible Erosion*

Table IV shows the slag composition after the pre-experiments, in which the last column (ΔMgO) represents the difference of MgO content in the slag before and after the pre-experiments, indicating the extent of erosion in the refractory lining. It is found that over 13 mass percent MgO was generated during the experiment for slag M1 even if no MgO was added to the initial slag, indicating that heavy erosion occurred. In addition, the amounts of MgO content in final slags M1 to M3 are close to each other for the same-basicity slag regardless of the amount of MgO in the initial slags and the approach to its saturated values as listed in Table III (11.12 pct).

Figure 1 shows the relationship between ΔMgO and the MgO content in the initial slags. ΔMgO gradually decreases when the MgO content in the initial slag increases, indicating that the degree of erosion of the crucible decreases as the content of MgO in the slag increases. Figure 2 shows the interface morphology between the slag and refractory lining for the M1 to M3 slags after the pre-experiments. An obvious light lining erosion from slag M1 to slag M3 can be observed, which is consistent with that in Table IV and Figure 1. In particular, there is almost no erosion of the refractory lining for slag M3, in which the MgO in the initial slag is close to the saturated value. Thus, it can be concluded that with an increase of MgO content in the initial slag, the erosion of the crucible refractory during the smelting process is much lower even if low-basicity slag is applied. According to the last column in Table III, the solubility of MgO increase much with slag basicity decrease, thus more MgO content should be added into the slag in the case of low-basicity slag smelting.

According to the pre-experimental results, the MgO content in the final slag is approximately equal to the saturation content of the slag no matter how much MgO content exists in the initial slag. Thus, in the following slag-steel equilibrium experiments, the MgO content is added to the saturated content for slags of different basicities to avoid heavy erosion of the lining. The saturated MgO content is calculated using the FactSage 7.2.[17]

B. *Effect of Basicity of Refining Slag on Inclusions and Steel Cleanliness*

Table V shows the final slag composition after the steel-slag equilibrium experiment. The content of MgO in the final slag is close to the content of MgO in the initial slag. This phenomenon indicates that the MgO crucible has almost not been eroded by the slag. It should be pointed out that CaF_2 contents in Table V were calculated by F element content determined by XRF. Table VI shows the content of T.O., S, and Als in steel samples after equilibrium experiments as refined by

Table IV. Composition of Final Slag in Pre-experiments, Mass Pct

No.	CaO	SiO_2	CaF_2	MgO	MnO	TiO_2	FeO	S	ΔMgO
M1	40.07	28.62	16.32	13.91	0.20	0.02	0.50	0.287	13.91
M2	41.96	29.97	15.69	11.73	0.19	0.03	0.22	0.177	6.73
M3	40.18	28.70	19.33	11.11	0.17	0.03	0.20	0.239	1.11

ΔMgO represents change of MgO content in slag after and before pre-experiments, the value of which reflects erosion extent of crucible.

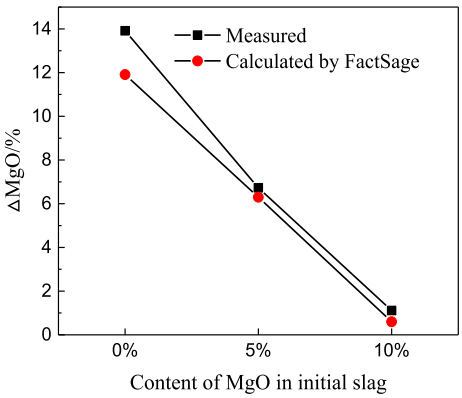

Fig. 1—Effects of different initial MgO content in slags with same basicity of 1.4 on refractory-lining erosion extent after pre-experiments.

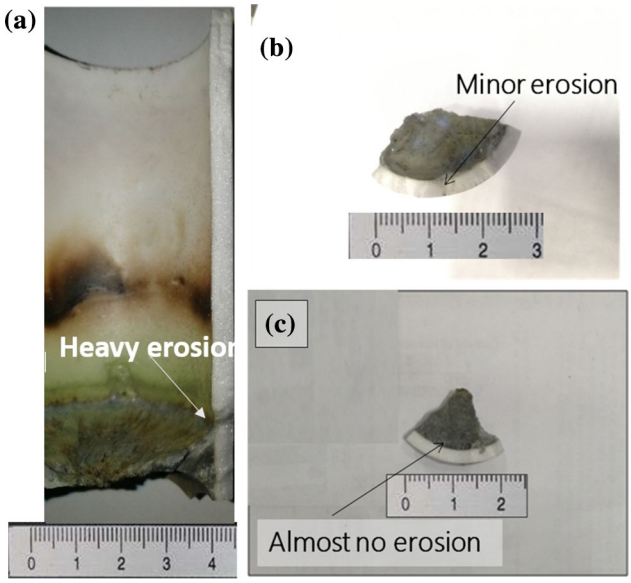

Fig. 2—Interface morphology between slag and refractory lining after pre-experiment: (*a*) slag M1, (*b*) slag M2, and (*c*) slag M3.

slags with different basicities. When the slag basicity increases, the T.O. content decreases from 19.6 to 4.1 ppm, while the Als content increases from 6.5 to 15.9 ppm.

Figure 3 shows the inclusion number density and the average diameter of steels R1 to R5. The number density of inclusions in steel is 15.57/mm^2 before the steel-slag equilibrium experiment. After the experiments, most of the inclusions in the steel float to the slag. As the basicity of the slag increases, the number of inclusions decreases, which is consistent with the changes in the total oxygen content of the steel shown in Table VI. The average diameter of the inclusions is about 3 μm regardless of the change in basicity of the slag.

Figure 4 shows the effect of the basicity of slag on the average composition of the inclusions in the steel samples. As the basicity of the slag increases, the content of MgO, Al_2O_3, and CaO in the inclusions increases. By contrast, the content of MnO in the inclusions decreases and disappears when the slag basicity is higher than 2.6. Interestingly, the content of (Al_2O_3 + MgO) in the inclusions increases linearly as the slag basicity increases. In addition, different types of inclusion can be achieved by slags of different basicity: SiO_2-MnO-Al_2O_3-based inclusions are generated when lower-basicity refined slag is applied, while SiO_2-CaO-Al_2O_3-based inclusions form when higher-basicity refined slag is applied. The former is deduced to form a spessartite phase, and the latter is inferred to generate an anorthite or gehlenite phase based on their composition. Table VII lists the melting points of these types of crystal phases as calculated by the FactSage 7.2[17]: spessartite has a much lower melting point than the latter two types of crystals. In particular, spessartite softens at the soaking temperature of 18 pct Cr-8 pct Ni stainless steel (1150 °C to 1250 °C), which is close to its melting point. Thus, it has much more favorable plasticity during the later rolling process. In addition, with the slag basicity increase, the MgO content also increase a lot thus it is much more likely to precipitate MgO·Al_2O_3 spinel phase within the inclusion that is with higher melting point (shown in Table VII) and more dangerous to steel quality.[1,2] Thus, it is favorable to improve the inclusion plasticity to achieve a MnO-SiO_2-Al_2O_3-based system inclusion for ultrathin stainless steel strips by low-basicity refining slag. In fact, researchers[2,6] discovered that SiO_2-MnO-Al_2O_3-based inclusions could deform significantly along the rolling direction during the rolling process. This supports the present conclusions. In addition, the experimental results suggest that MgO saturated slag do not have extra negative effects on inclusion plasticity, in particular in the case of low-basicity slag.

Table V. Composition of Final Slag in Steel-slag Equilibrium Experiments, Mass Pct

No.	R	CaO	SiO_2	CaF_2	Al_2O_3	MgO	MnO	FeO	S
R1	1	31.80	31.80	15.89	0.62	18.35	0.52	0.22	0.22
R2	1.4	42.51	30.36	12.61	1.03	12.31	0.26	0.28	0.25
R3	1.80	47.09	26.16	18.26	0.47	7.13	0.10	0.08	0.30
R4	2.20	54.84	24.93	10.03	2.27	7.33	0.05	0.02	0.22
R5	2.60	55.94	21.51	15.42	1.35	5.11	0.03	0.02	0.26
R6	3.00	58.54	19.51	15.24	1.71	4.25	0.04	0.03	0.28

Table VI. Effect of Slag Basicity on T.O., S, and Als in Steel After Experiment

Slag No.	T.O. (ppm)	S (ppm)	Als (ppm)
R1	19.6	14.2	6.5
R2	13.2	12.1	6.2
R3	11.1	9.6	6.3
R4	6.6	5.9	12.6
R5	4.7	4.6	12.4
R6	4.1	4.3	15.9

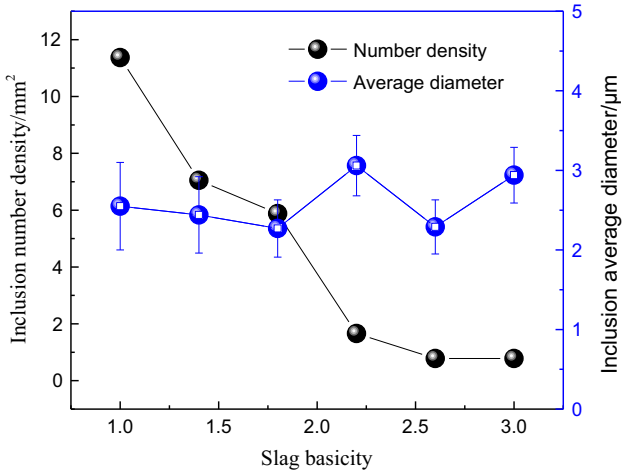

Fig. 3—Effect of slag basicity on number density and average diameter of inclusions.

C. *Thermodynamic Analysis*

Since the 18 pct Cr-8 pct Ni stainless steel is a Si-killed steel, its [O] is determined by the [Si]-[O] reaction in equilibrium with SiO_2 of top slag after steel-slag equilibrium achievement. The chemical reaction is expressed as follows, in which the data of standard Gibbs free energy is referred to Reference 18.

$$[\mathrm{Si}] + 2[\mathrm{O}] = (\mathrm{SiO_2}), \Delta G^{\Theta} = -576440 + 218.2T, \quad [1]$$

When the reaction achieves equilibrium, its equilibrium constant (K) and the oxygen activity in molten steel ($a_{[O]}$) can be expressed as Eqs. [2] and [3], respectively:

$$\log K = \log \frac{a_{\mathrm{SiO_2}}}{a_{[\mathrm{Si}]} \cdot a_{[\mathrm{O}]}^2} = \frac{30110}{T} - 11.4 \quad [2]$$

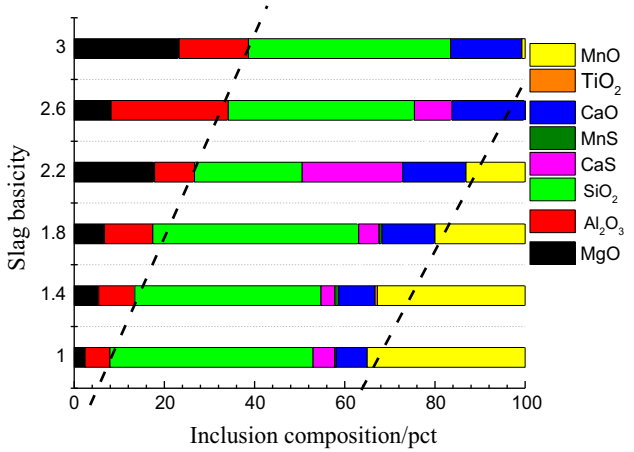

Fig. 4—Effect of slag basicity on average composition of inclusions.

$$a_{[\mathrm{O}]} = \sqrt{\frac{10^{\left(\frac{30110}{T} - 11.4\right)} \cdot a_{\mathrm{SiO_2}}}{a_{\mathrm{Si}}}} \quad [3]$$

where T is the Kelvin temperature, a_{SiO_2} is the activity of SiO_2 in slag relative to pure quartz, and $a_{[Si]}$ and $a_{[O]}$ are the activities of [Si] and [O] in liquid steel relative to the 1 pct standard state. In the present study, a_{SiO_2} is calculated by the ion-molecule coexistence theory (IMCT), as shown in Figure 5. The precision of IMCT was frequently verified by researchers, in particular in the case of predicting the component activities of multicomponent slag.[19–21] The slag for smelting 18 pct Cr-8 pct Ni stainless steel is CaO-SiO_2-Al_2O_3-MgO-MnO-FeO-TiO_2-Cr_2O_3-CaF_2 nine component system. In the calculations, given that there are 39 structural units, including simple ion couples, simple molecules and complex molecules, in the molten slags. In addition, the reactions of forming complex molecules are considered in chemically dynamic equilibrium between bonded ion couples and simple molecules. Nine equations with nine variables (component activities) can be deduced according to their equilibrium constants and the law of mass conservation. The unique solution can be obtained by Matlab software. The detailed calculations are included in our previous work.[19,21]

The activity coefficients f_{Si} and f_O are calculated by the Wagner formula in Eq. [4], where e_i^j is the first-order activity interaction coefficient of elements j to i relative to the diluted solution. These values are listed in Table VIII. It should be pointed out that the activity interaction coefficients applied in the present calculations are selected from those measured based on Fe-Cr-Ni stainless steel hot metal, or those were confirmed applicable for the 18 pct Cr-8 pct Ni stainless steel. The calculated results in Figures 6 and 7 also suggest the high applicability of these data.

$$\lg f_i = \sum e_i^j [\text{mass pct } j] \qquad [4]$$

Figure 5 shows the calculated activities of SiO_2 and Al_2O_3 in the slag with different basicities. The activity of SiO_2 in the slag decreases sharply (from 6.4×10^{-3} to 7.3×10^{-5}) as the basicity of the slag increases. This might result in an obvious decrease in the oxygen activity of steel according to Eq. [3]. As the steel samples have similar primary compositions, the activity coefficients of oxygen are similar to each other. It can be deduced that the dissolved [O] in molten steel will also decrease correspondingly as the slag basicity increases.

Table IX lists the comparison of T.O. measured in present experiments and those measured by some other researchers. Compared to Ren *et al.*[14] and Park *et al.*[11] results, the largest difference is that MgO contents in the present slag were nearly saturated, while MgO contents in Ren *et al.*[14] and Park *et al.*[11] were approximating 3 pct. With the same slag basicity, the T.O. in presents experimental are lower than T.O.s in Ren *et al.*'s and Park *et al.*'s experiments. In addition, the present results are also confirmed that T.O. can be further decreased with larger slag basicity, in particular, the T.O.s lower than 5 ppm in the case of slag basicity higher than 2.2. Suzuki *et al.*[22,23] experimental results had much higher T.O.s since there were no top slag in their experiments. Hence, it can be obtained MgO saturated slag do not have extra negative effects on inclusion plasticity and steel cleanliness but it can effectively prevent the refractory erosion during the smelting process, in particular in the case of low-basicity slag.

Figure 6 shows the evolution of the measured T.O. and [O] calculated by the [Si]-[O] equilibrium with slags of different basicities. The measured T.O. and calculated [O] have very similar tendencies as the slag basicity

Table VII. Melting Points of Typical Crystal Phases

Crystal Phase	Component	Melting Point (°C)	Properties
Spessartite	$Mn_3Al_2Si_3O_{12}$	1208	Plasticity
Anorthite	$CaAl_2Si_2O_8$	1555	Crisp
Gehlenite	Ca_2AlSiO_7	1595	Crisp
Spinel	$MgO{\cdot}Al_2O_3$	2108	Crisp/hard

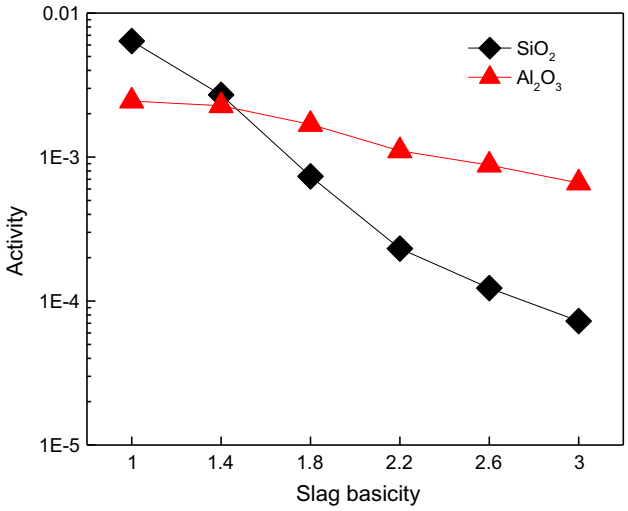

Fig. 5—Activity of SiO_2 and Al_2O_3 in final slag with different basicity calculated by IMCT.

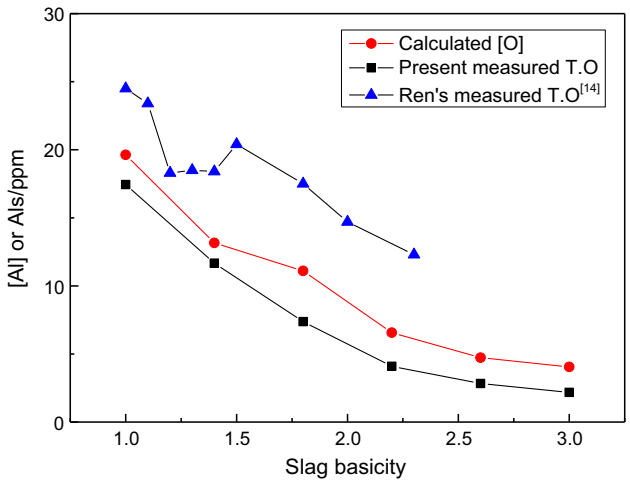

Fig. 6—Measured T.O. and [O] calculated by [Si]-[O] equilibrium refined by different basicity slag.

Table VIII. Activity Interaction Coefficients Applied to Present Calculations

e_i^j	C	Si	Mn	P	S	Cr	Ni
Si	0.18[18]	0.11[18]	0.002[18]	0.11[18]	0.056[18]	− 0.021[22]	− 0.009[23]
Al	0.091[18]	0.0056[18]	0.035[18]	—	0.03[18]	0.03[1]	− 0.029[24]
O	− 0.45[18]	− 0.066[18]	− 0.021[18]	0.07[18]	− 0.133[18]	− 0.033[23]	0.006[23]

varies; both decrease as the basicity of the slag increases. It should be noted that the content of T.O. is the sum of the dissolved oxygen in molten steel [O] and oxygen in the inclusions. As the slag-steel reaction time is long enough in the experiments, inclusions in molten steel can fully float up and be absorbed by the slag. Therefore, the content of dissolved oxygen is a major part of the T.O. in the steel samples. The [O]s are only several ppm lower than the T.O.s, indicating a favorable steel cleanliness in these steel samples. Moreover, the agreement between the calculated [O] and measured T.O. implies that the content of dissolved oxygen in the stainless steel is indeed controlled by the [Si]-[O] equilibrium. The dissolved [Al] in the liquid steel at equilibrium is usually determined by the following reaction shown in Eq. [5]. The dissolved [Al] can be deduced from Eqs. [6] through [8]. $a_{Al_2O_3}$ is also calculated by IMCT as a_{SiO_2}, as shown in Figure 6.

$$3[Si] + 2(Al_2O_3) = 3(SiO_2) + 4[Al] \log K^{\theta} = -\frac{16800}{T} - 1.96 \quad [5]$$

$$\log K = \log \frac{a^2_{Al_2O_3} \cdot a^3_{[Si]}}{a^3_{SiO_2} \cdot a^4_{[Al]}} \quad [6]$$

$$\log a_{Al} = \frac{2 \log a_{Al_2O_3} + 3 \log a_{[Si]} - 3 \log a_{SiO_2} - \log K}{4} \quad [7]$$

$$[\text{Pct Al}] = a_{[Al]}/f_{Al} \quad [8]$$

Figure 7 shows a comparison between the calculated [Al] by Eq. [8]and measured Als under different slag basicities. In addition, other researchers' experimental results for similar slag compositions are listed in the figure for comparison. Notably, the measured Als by ICP-MS and calculated [Al] in liquid steel are somewhat different; however, these are typically considered equal to each other. One can see that both the measured Als and the calculated ones increase as the slag basicity increases. To some extent, the measured Als and [Al] calculated by the steel-slag equilibrium are consistent in their tendency of evolution, although some deviations appear between the calculated [Al] and the measured ones when the slag basicity is higher. This is likely owing to the effects of some other components in the slag and liquid steel. As shown in Figure 5, with slag basicity increase from 1.0 to 3.0, the activity of SiO_2 in slag

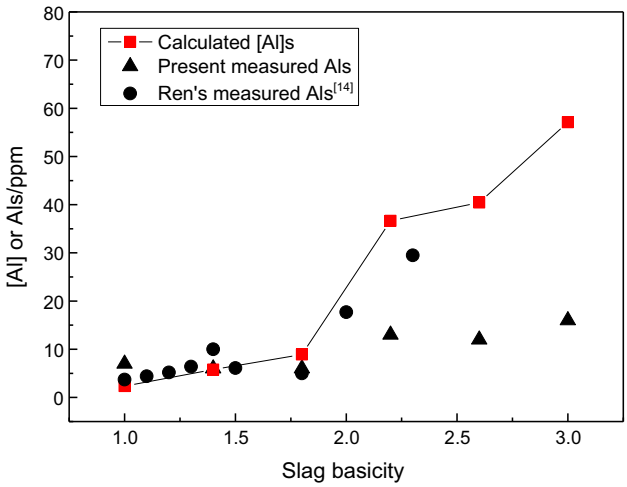

Fig. 7—Content of measured Als and [Al] calculated by [Al]-(SiO_2) equilibrium.

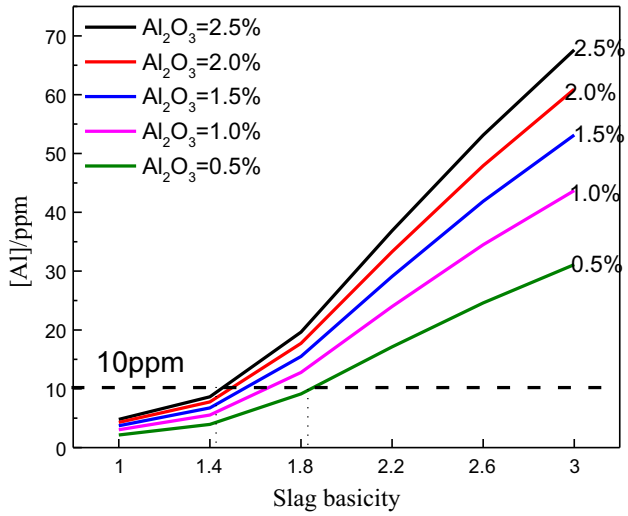

Fig. 8—Effect of content of Al_2O_3 in different basicity slag on content of [Al] in steel.

Table IX. Comparison of Experimental Results on Stainless Steel by Different Authors

Authors	Slag Basicity	Als in Steel (ppm)	T.O. (ppm)	Note
Present	1.0–3.0	6.5–15.9	4.05–19.63	MgO saturated
Ren *et al.*[14]	1.0–2.3	3.7–29.5	12.3–23.4	MgO ≈ 3 pct
Park *et al.*[11]	1.0–2.0	9.5–32	9.0–15.0	MgO ≈ 3 pct Al_2O_3 30–52 pct
Suzuki *et al.*[22]	no slag,	no Als content, Si 0.4–1.0 pct	66–415	silica crucible, Cr 5–25 pct
Suzuki *et al.* [23]	no slag,	no Als content, Si ≈ 0.4 pct	66–415	silica crucible, Ni 4–20 pct

decrease from 6.4×10^{-3} to 7.3×10^{-5}, while activity of Al_2O_3 decrease from 2.5×10^{-3} to 6.6×10^{-4}, indicating that SiO_2 activity decreases much more rapidly than that of Al_2O_3 activity, which facilitates reaction [5] and results in the Als increase with slag basicity increase.

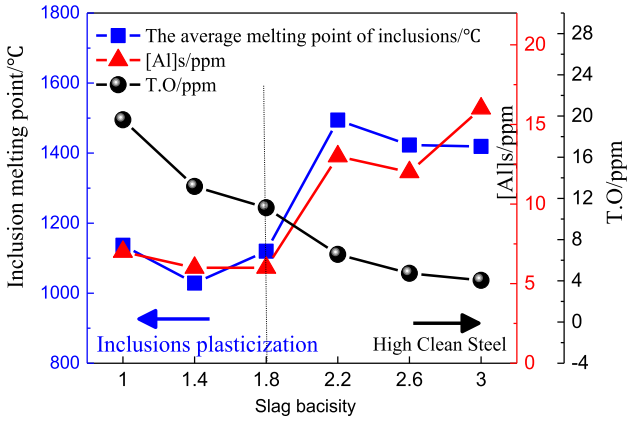

Fig. 9—Effect of slag basicity on average melting point of inclusion and content of T.O. and Als in steel.

Figure 8 shows the effect of the content of Al_2O_3 in slag on the content of [Al] in steel based on a quantitative thermodynamic calculation. When the basicity of the slag is constant, the [Al] in the steel increases when the content of Al_2O_3 in the slag increases from 0.5 pct to 2.5 pct. In particular, the increasing trend for [Al] content in the steel becomes more obvious when the basicity of the slag is higher. This indicates that to reduce the content of [Al] in steel, the content of Al_2O_3 in slag should be as low as possible. Moreover, it can be deduced that slag with lower basicity can accommodate more Al_2O_3 content in the slag to achieve the same low [Al] content in steel. For example, to control the content of [Al] in steel to under 10 ppm, the content of Al_2O_3 in slag should be below 0.5 pct when the basicity of the refining slag is 1.8, while the content of Al_2O_3 in the slag can increase to 2.5 pct when the slag basicity is 1.4. Since during these experiments no deoxidizer was added in steel at all, the origination of Als increment in steel is considered due to reduction of Al_2O_3 in slag by Si in steel by the chemical reaction [5]. In addition, thermodynamic results in Figure 8 show that Als in steel increase with Al_2O_3 content increasing in slag, which further verifies the origination of Als is from reduction of Al_2O_3 of slag. It should be noted that the source of Als in steel during industrial process is somewhat different from that in laboratory-scale

Table X. Slag Composition at End of LF Refining, Mass Pct

No	R	CaO	SiO_2	CaF_2	MgO	Al_2O_3	Cr_2O_3	MnO	FeO
T1	1.53	46.38	30.27	12.19	7.74	2.09	0.27	0.32	0.26
T2	1.75	45.92	26.27	16.69	6.68	2.20	0.10	0.07	0.08

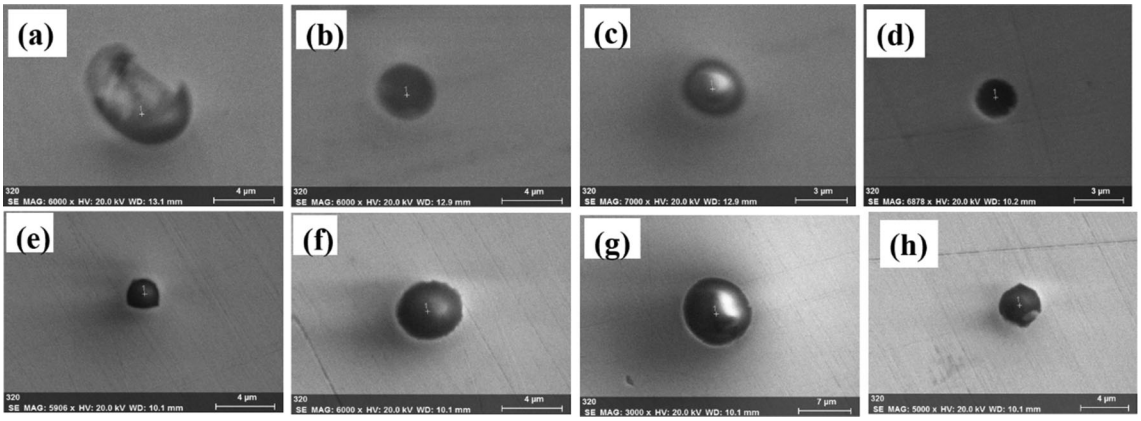

Fig. 10—Typical inclusion morphologies and corresponding composition in the continuous-casting slab, (*a*) to (*d*) Heat T1 and (*e*) to (*h*) Heat T2.

Table XI. Steel Composition at End of LF Refining, Mass Pct

No.	C	Si	Mn	P	S	Cr	Ni	Als (ppm)	T.O. (ppm)
T1	0.048	0.42	1.16	0.0323	0.0015	18.00	8.17	9	35.3
T2	0.047	0.43	1.20	0.032	0.0012	18.15	8.01	19	33.5

experiment since the deoxidizing alloys, such as ferrosilicon and manganeisen, would introduce much aluminum to the steel that is one of the main origination of Als in steel, thus the quality of deoxidizing alloys is also very key to improve inclusion plasticity in actual industrial process.

The effects of slag basicity on the average melting point of the inclusions and the content of T.O. and Als in steel is shown in Figure 9. The inclusion melting points are the average values of all melting points of inclusions in one specimen as calculated by database FactSage 7.2.[17] There is also an interesting phenomenon in that the content of Als in steel almost corresponds to the melting point of the inclusions. This indicates that it is extremely important to improve the plasticity of the inclusion to reduce the content of Als in 18 pct Cr-8 pct Ni stainless steel. In the meantime, the slag basicity plays a key role since it affects the Als directly, as shown in Figure 7. On the other hand, the T.O. in steel has a tendency opposite to that of the Als content and inclusion melting point. Hence, two strategies can be applied in the production of stainless steel: higher-cleanliness steel can be produced by improving the basicity of the slag, while the non-metallic inclusion plasticity can be increased by decreasing the basicity of the slag. Different compositions of slag can be selected according to the specific requirements of the final product. In addition, with refining slag basicity between 1.4–1.8 and Als lower than 10 ppm, a relatively favorable inclusion plasticity and high steel cleanliness can be obtained. To obtain a lower content of Als in the steel and a favorable inclusion plasticity, a low-basicity slag should be employed.

D. *Industrial Trial Results*

Tables X and XI show the final slag and liquid steel compositions for the two heats at the end of LF refining, respectively. There was almost no extra erosion to the refractory lining of the ladle even when lower-basicity slag was used in the testing heat because a proper amount of light-burning dolomite was added. In addition, the T.O. and S content in testing heat T1 was 35.3 ppm and 15 ppm, respectively, only slightly higher than that in conventional heat T2, while the Als in heat T1 (9 ppm) was much lower than that in the heat T2 (19 ppm).

Figure 10 shows some typical inclusion morphologies in the slab samples in heat T1 and heat T2. In addition, inclusion compositions are listed in Table XII. Morphologies of inclusions in the two heats are main spherical and their size are mainly lower than 10 μm, But their inclusion compositions are obvious different. The inclusions in slab of heat T1 are mainly composed of MnO, SiO_2 and Al_2O_3, as well as small amount of CaO, in which the ratio of inclusions in heat T1 with mass fraction of (SiO_2 + MnO + Al_2O_3 + MgO) larger than 80 pct and with CaO lower than 10 pct is 93.1 pct (219/235). On the contrary, CaO contents of the inclusions in slab of heat T2 are much more, while the MnO content are much less. Furthermore, the Al_2O_3 content in the inclusion also increase obviously as well as MgO and/or TiO_2. The ratio of inclusions in heat T2 with mass fraction of (SiO_2 + CaO + Al_2O_3 + MgO) larger than 80 pct and with MnO lower than 10 pct is 85.4 pct (170/199). Hence, it can conclude that the inclusions in heat T1 are SiO_2-MnO-Al_2O_3 based and that in heat T2 are CaO-SiO_2-Al_2O_3 based in composition.

Table XII. Composition of Inclusion in Fig. 10, Mass Pct

No.	CaO	SiO_2	MgO	Al_2O_3	MnO	TiO_2
(a)	0	25	0	15	51	9
(b)	4	37	0	18	41	0
(c)	0	43	0	19	38	0
(d)	9	44	7	15	26	0
(e)	13	13	15	51	6	2
(f)	21	25	10	34	5	5
(g)	41	29	9	19	1	0
(h)	23	31	5	27	11	0

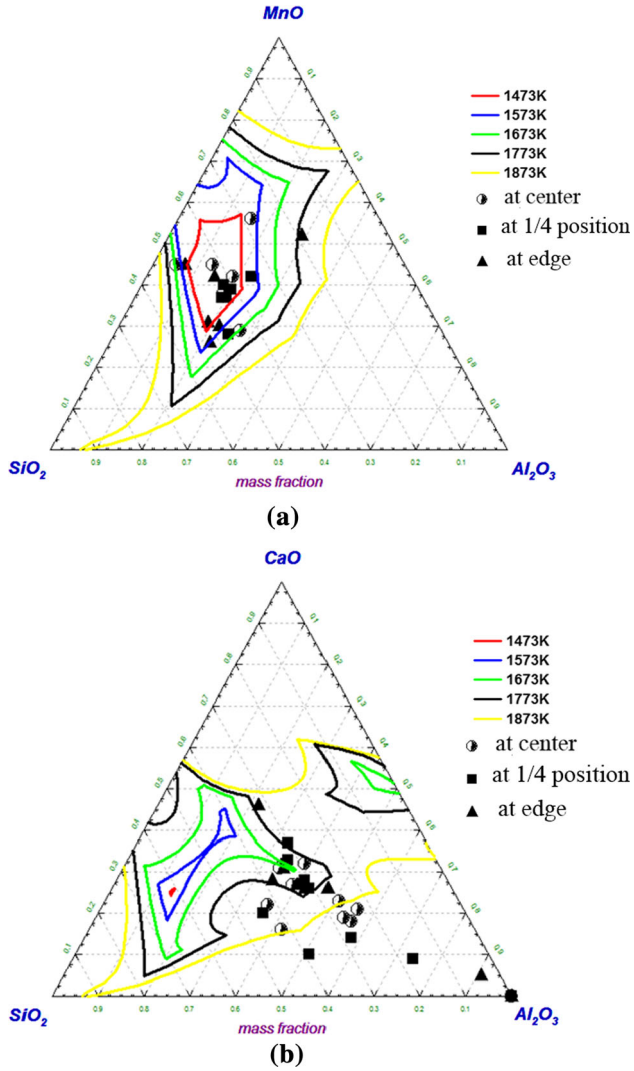

Fig. 11—Composition of inclusions in continuous-casting slab (*a*) T1 and (*b*) T2 projected in isothermal SiO_2-MnO-Al_2O_3 and SiO_2-CaO-Al_2O_3 ternary-phase diagrams.

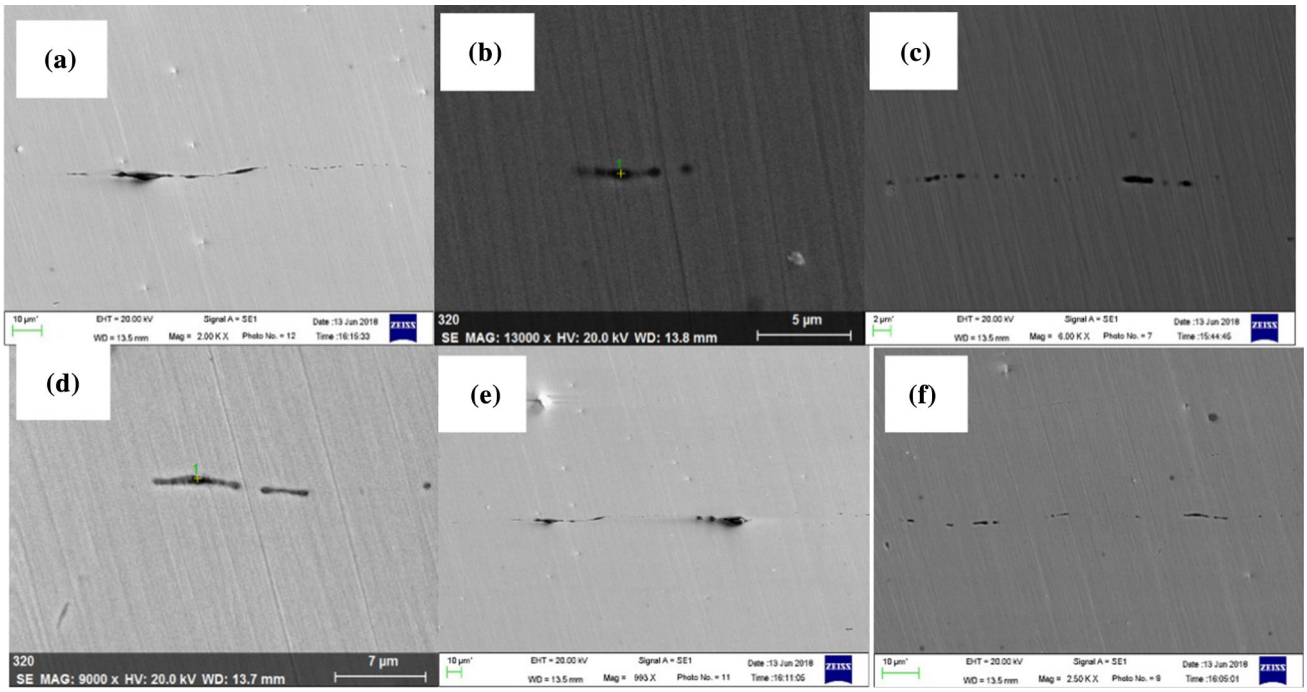

Fig. 12—Some typical deformed inclusions (*a* to *f*) during corresponding cold-rolled strip of heat T1 with a thickness of 0.1 mm.

Figure 11 shows the composition of the inclusions in the continuous-casting slabs of T1 and T2 projected in isothermal SiO_2-MnO-Al_2O_3 and SiO_2-CaO-Al_2O_3 ternary-phase diagrams, respectively. Different symbols indicate the inclusion composition at different positions at central line along the width direction within one slab. Most of the inclusion compositions in heat T1 locate at melting points lower than 1573 K (1300 °C), while the majority of the inclusions in heat T2 have melting points higher than 1673 K (1400 °C) and some high melting point Al_2O_3 and MgO·Al_2O_3 spinel inclusions were also observed(as shown in Al_2O_3 corner of Figure 11(b)). Hence, favorable inclusion plasticity as well as relatively high steel cleanliness is achieved by controlling the lower slag basicity and low Als content in steel. This is in good agreement with the laboratory-scale experiment and thermodynamic calculated results.

The composition of the inclusions in the slab is SiO_2-MnO-Al_2O_3 ternary-based system, and thus the composition of the inclusions is plotted on the ternary-phase diagram of SiO_2-MnO-Al_2O_3 with isotherms. The melting point of most inclusions in the slab is less than 1300 °C, indicating they are likely to softening during the rolling temperature. Figure 12 represents some typical inclusion morphologies in corresponding cold-rolled strips of heat T1, in which most of them are well deformed along the rolling directions, which confirms the inclusions are of favorable plasticity.

IV. CONCLUSIONS

In this study, laboratory-scale experiments on Si-deoxidized 18 pct Cr-8 pct Ni stainless steel equilibria with different slag compositions were carried out. Thermodynamic analysis was also performed by applying the ion-molecule coexistence theory and thermodynamic database FactSage to investigate how the refining slag composition affects the non-metallic inclusion plasticity and steel cleanliness. In addition, industrial tests were conducted to validate the results. The following conclusions were reached:

First, the content of MgO in slag should be nearly saturated in composition to avoid too-heavy erosion to the MgO-based refractory lining for low-basicity slag. In addition, MgO saturated slag did not have extra negative effects on inclusion plasticity and steel cleanliness.

Second, with an increase in the basicity of slag, the inclusions in steel evolved from SiO_2-MnO-Al_2O_3-based to SiO_2-CaO-Al_2O_3-based ones, and their plasticity decreased. Meanwhile, the T.O. in steel decreased, while the content of Als in the steel increased correspondingly.

Finally, low slag basicity, low Al_2O_3 content in the slag and low Als content in liquid steel were in favor to generate to more MnO-SiO_2-Al_2O_3-type inclusion and increase plasticity of non-metallic inclusions in steel, while a higher slag basicity was beneficial to promoting

steel cleanliness. Thermodynamic analysis, laboratory-scale experimental and industrial trials verified that a favorable inclusion plasticity and relatively high steel cleanliness could obtain when refining slag with a basicity between 1.4 and 1.8 and Als lower than 10 ppm.

ACKNOWLEDGMENTS

The authors express their gratitude to the National Science Foundation for Young Scientists of China (5170402), China Postdoctoral Fund (2018M630071), Fundamental Research Funds for the Central Universities (FRF-TP-19-030A2, FRF-TP-16-079A1), and the Joint Funds of the National Natural Science Foundation of China (U1560203) for their kind financial support.

REFERENCES

1. J.H. Park and H. Todoroki: *ISIJ Int*., 2010, vol. 50, pp. 1333–46.
2. J.H. Park and Y. Kang: *Steel Res. Int*., 2017, vol. 88, p. 1700130.
3. H. Suito and R. Inoue: *ISIJ Int*., 1996, vol. 36, pp. 528–36.
4. Z.L. Xue and Z.B. Li: *J. Iron Steel Res. Int*., 2003, vol. 10, pp. 38–44.
5. L.F. Zhang and G.T. Brian: *ISIJ Int*., 2003, vol. 43, pp. 271–91.
6. K.P. Wang, M. Jiang, X.H. Wang, Y. Wang, H.Q. Zhao, and Z.M. Cao: *Metall. Mater. Trans. B*, 2015, vol. 46B, pp. 2198–2207.
7. J. Guo, S.S. Cheng, and Z.J. Cheng: *ISIJ Int*., 2013, vol. 53, pp. 2142–51.
8. J.H. Park: *Mater. Sci. Eng. A*, 2008, vol. 472, pp. 43–51.
9. H.L. Yang, J.S. Ye, X.L. Wu, Y.S. Peng, Y. Fang, and X.B. Zhao: *Metall. Mater. Trans. B*, 2016, vol. 47B, pp. 1435–44.
10. Q. Wang, L.J. Wang, J. Zhai, J.M. Li, and K.C. Chou: *Metall. Mater. Trans. B*, 2017, vol. 48B, pp. 564–72.
11. J.S. Park and J.H. Park: *Metall. Mater. Trans. B*, 2014, vol. 45B, pp. 953–60.
12. O. Wijk and V. Brabie: *ISIJ Int*., 1996, vol. 36, pp. S132–35.
13. Y.B. Kang and H.G. Lee: *ISIJ Int*., 2004, vol. 44, pp. 1006–15.
14. Y. Ren, L.F. Zhang, W. Fang, S.J. Shao, J. Yang, and W.D. Mao: *Metall. Mater. Trans. B*, 2016, vol. 47B, pp. 1024–34.
15. K. Mizuno, H. Todoroki, M. Noda, and T. Tohge: *Iron Steelmak*., 2001, vol. 28 (8), pp. 3–101.
16. M. Jiang, X.H. Wang, B. Cheng, and W.J. Wang: *ISIJ Int*., 2010, vol. 50, pp. 95–104.
17. C.W. Bale, E. Bélisle, P. Chartrand, S.A. Decterov, G. Eriksson, A.E. Gheribi, K. Hack, I.H. Jung, Y.B. Kang, J. Melançon, A.D. Pelton, S. Petersen, C. Robelin, J. Sangster, P. Spencer, and M.A. Van Ende: *ISIJ Int*., 2016, vol. 54, pp. 35–53.
18. The Japan Society for the Promotion of Science: *Steelmaking Data Sourcebook*, Gordon & Breach Science Publishers, New York, 1988.
19. S.C. Duan, X.L. Guo, H.J. Guo, and J. Guo: *Ironmak. Steelmak*., 2017, vol. 44, pp. 168–84.
20. X.M. Yang, J.Y. Li, M. Zhang, G.M. Chai, and J. Zhang: *Metall. Mater. Trans. B*, 2014, vol. 45B, pp. 2118–37.
21. S.W. Han, J. Guo, X.R. Chen, H.J. Guo, and S.C. Duan: *Iron Steel*, 2018, vol. 53, pp. 47–52 (in Chinese).
22. K. Suzuki, S. Ban-ya, and M. Hino: *ISIJ Int*., 2001, vol. 41, pp. 813–17.
23. K. Suzuki, S. Ban-ya, and M. Hino: *ISIJ Int*., 2002, vol. 42, pp. 146–49.
24. H. Ohta and H. Suito: *ISIJ Int*., 2003, vol. 43, pp. 1293–1300.